BULLETIN OF THE POLISH ACADEMY OF SCIENCES
TECHNICAL SCIENCES, Vol. 69(6), 2021, Article number: e137987
DOI: 10.24425/bpasts.2021.137987

Research on stability and sensitivity of the rotating machines with overhung rotors to lateral vibrations

Tomasz SZOLC * **and Robert KONOWROCKI**

Institute of Fundamental Technological Research of the Polish Academy of Sciences, ul. Pawińskiego 5B, 02-106 Warsaw, Poland

Abstract. The rotating machines with overhung rotors form a broad class of devices used in many types of industry. For this kind of rotor machine in the paper, there is investigated an influence of dynamic and static unbalance of a rotor, parallel and angular misalignments of shafts, and inner anisotropy of rigid couplings on system dynamic responses. The considerations are performed through a hybrid structural model of the machine rotor-shaft system, consisting of continuous beam finite elements and discrete oscillators. Numerical calculations are carried out for parameters characterizing a heavy blower applied in the mining industry. The main goal of the research is to assess the sensitivity of the imperfections mentioned above on excitation severity of rotor-shaft lateral vibrations and motion stability of the machine in question.

Key words: overhung rotor-shaft; lateral vibrations; stability and sensitivity analysis; system imperfections.

1. INTRODUCTION

The rotating machines with overhung rotors form a broad class of devices used in many types of industry. These include pumps, compressors, fans, blowers, beater mills and many more. Most of them are characterized by a similar structure in the form of a relatively short shaft with a heavy rotor mounted outside the bearing surfaces. Electric motors usually drive them by means of rigid or flexible couplings. Results of experimental measurements registered on real objects show that balancing errors of their rotors, worn rolling bearing raceways, rotor-to-stator rubbing, and various inaccuracies in a connection of the machine with the motor cause significant lateral vibrations of the entire rotating system. Because of these reasons, the rotating machines with overhung rotors became an object of numerous dynamic investigations during the last decade. In [1], nonlinear whirl effects are studied for the overhung rotor model of Crandall and Brosens. In [2], a dynamic interaction of the unbalanced flexible overhung rotor with ball bearings is investigated. Dynamic responses of an elastically supported overhung rotor with uncertain parameters are studied in [3]. An influence of friction during contact between the rotor and stator on rotor-shaft forward and backward precession is analyzed in [4] on the example of a machine with an overhung rotor.

For this class of rotor machines, in the paper presented here, there is investigated an influence of dynamic and static unbalance of rotors, parallel and angular misalignments of shafts, and inner anisotropy of rigid couplings on a system dynamic responses. The considerations are performed by means of a hybrid structural model of the machine rotor-shaft system, which consists of continuous beam finite elements and discrete oscillators. The main research focuses on sensitivity to imperfections and stability analyses, including applying the harmonic balance method for a parametric problem. Numerical calculations are carried out for parameters characterizing a very representative real object, i.e., a heavy blower applied in the mining industry.

2. MODELLING OF TYPICAL IMPERFECTIONS OF THE ROTOR MACHINES WITH OVERHUNG ROTORS

Rotor machines with overhung rotors are characterized by two basic features, which usually significantly influence magnitudes of lateral/bending vibrations affecting these devices. The first of these features is a very heavy overhung rotor, the mass of which often can be up to ten times greater than that of the shaft itself. The second important feature is the presence of a rigid or flexible coupling connecting the rotor shaft with the shaft of the driving motor. These characteristic properties clearly distinguish these machines from a very wide group of various rotating machines, also experiencing several types of onerous mechanical vibrations. Namely, these features determine additional, specific sources of excitation, which in the case of rotating machines of different types often become secondary or even insignificant. The vibration sources important for the rotor machines with overhung rotors include:

1. dynamic unbalance of the rotor, which most often may be caused by its improper mounting on the shaft or incorrectly positioned blades;
2. mutual misalignment, parallel or angular, of the rotor shaft in relation to the remaining shaft segments and the rotor of the driving motor;

*e-mail: tszolc@ippt.pan.pl

Manuscript submitted 2021-04-06, revised 2021-05-22, initially accepted for publication 2021-05-28, published in December 2021

3. anisotropy of elastic properties of couplings in the form of the so-called inner anisotropy, caused by errors in the manufacture or assembly of couplings, or most often, plastic deformations of faces of the coupling discs and their screw connections, which gradually increase during operation.

There are also other sources of excitations, typical for most rotating machines, such as static unbalances of rotors, i.e., the overhung rotor itself and the rotor of the driving motor. Moreover, additional excitations are often caused, e.g., by cracked or bowed rotor-shafts, rotor-to-stator rub-impacts, and damage of bearing raceways, especially rolling bearings. However, it should be noted here that the mentioned above kinds of imperfections will not be considered in this study because they are also common to a wide variety of other rotating machines, and not particularly to the rotating machines with overhung rotors.

2.1. Modelling of the dynamic unbalance of the overhung rotor

From the viewpoint of fundamentals of dynamics of a rigid body, a dynamic unbalance consists of a rotation of its central principal axes of inertia by a slight angle with respect to the center of mass of the rigid body so that one of these axes do not coincide with the axis around which this body rotates. This situation has been illustrated schematically in Fig. 1.

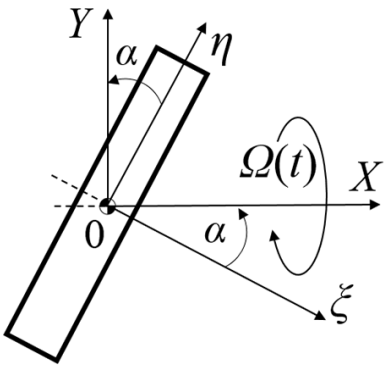

Fig. 1. Dynamic unbalance of the rigid body representing a rotor

Generally, as commonly defined, e.g., in [5], in cases of long, slender rotors, the dynamic unbalance is equivalent to two static unbalance forces with amplitudes proportional to a square of the rotor-shaft current rotational speed. These forces act in two specified planes perpendicular to the rotation axis, and their temporary values mutually fluctuate in antiphase so that they yield a moment of a couple of forces, which causes a dynamic bending of the entire rotor-shaft.

Overhung rotors, however, usually belong to the class of so-called "narrow rotors", and thus their dynamic unbalance ought to be modelled in another way. Namely, by transforming the inertia tensor of a rigid body that represents an overhung rotor to the inertial, non-rotating coordinate system $Oxyz$, determining next the total kinetic energy of this rigid body in a spherical motion, by means of the components of this tensor and using Lagrange's equations of the second kind one gets components of the bending moments $M_z(t)$ and $M_y(t)$ forcing lateral/bending vibrations of the rotor shaft, respectively in the vertical plane Oxy and the horizontal plane Oxz:

$$\begin{aligned} M_z(t) &= \Omega^2(t)\left[\frac{1}{2}\left(I_\xi - I_\eta\right)\sin(2\alpha)\right]\cos\Theta(t), \\ M_y(t) &= \Omega^2(t)\left[\frac{1}{2}\left(I_\xi - I_\eta\right)\sin(2\alpha)\right]\sin\Theta(t), \end{aligned} \tag{1}$$

where: $\Theta(t) = \int_0^t \Omega(\tau)\mathrm{d}\tau$,

$\Omega(t)$ is the current rotational speed around the Ox axis, and I_ξ, I_η are the two out of three central, main mass moments of inertia of the rigid body. These excitations are harmonically variable with a synchronous frequency 1X and have a form analogous to excitation due to static unbalances. It should be emphasized that if the rigid body in question represents a heavy overhung rotor, and I_ξ is its polar mass moment of inertia with respect to the rotation axis Oξ in the rotating coordinate system, and I_η is the diametrical mass moment of inertia of this rotor with respect to the axis perpendicular to Oξ, as illustrated in Fig. 1, then despite the aforementioned low value of angle α, the product $0.5\cdot\left(I_\xi - I_\eta\right)\cdot\sin(2\cdot\alpha)$ can be large enough to generate excitation magnitudes comparable or much greater than those caused by realistic static unbalances.

2.2. Modelling of the rotor-shaft misalignments

The individual sections of shafts of the rotating machinery drive systems are generally interconnected by couplings of different types, with different properties depending on the specific structure of the entire device. Both during an assembly process and due to changes taking place during operation, there is often a lack of perfect mutual coaxiality of these shafts in the form of their mutual parallel or angular displacement. In these cases, the properties of couplings joining these shafts have a huge impact on static and dynamic loads that occur during the device's operation. Although this phenomenon has been observed since the beginning of the drive systems of various types of machines, devices and vehicles, scientific research on misalignments of shafts and rotors was intensified at the end of the 20$^{\text{th}}$ century, and especially in the two decades of the current century. This is confirmed by numerous publications from that period, for example [6–11].

Rigid couplings in the form of flanges connected with bolts directly or through appropriate sleeves or by the use of lamella discs have a special influence on the misalignment of shafts. Then, such a screw connection significantly affects the nature of the load of an entire rotating drive system. In the case of a perfectly concentric connection of both coupling flanges mounted on mutually misaligned sections of the shafts, their static bending occurs, thus determining a geometric shape of the isostatic deflection line of the entire rotor-shaft system. This results in the action of only constant additional reaction forces of bearing supports, sometimes very significant, but without variable components inducing vibrations, [7, 9]. It should be noted here that in such situations, the parallel misalignment

of shafts connected in this way transforms into their angular misalignment. It usually occurs as a result of degradation of bearing supports in the form of "settling" on foundations, which increases during the operation of a given object.

A completely different effect on the parallel misalignment of shafts connected by a rigid coupling is a lack of mutual concentricity of the circuits formed by rims of the bolts on both flanges, see Fig. 2a. This occurs most often as a result of mounting inaccurately aligned sections of shafts in their supports. Then, most often, these shafts do not experience initial static deformations. However, the resulting mutual parallel displacement of their geometric axes by a finite value of δ_k during rotational motion becomes a source of harmonic excitation of a kinematic type with a synchronous frequency 1X for transverse loads that induce bending vibrations of the entire shaft line and with a double synchronous frequency 2X for torsional loads that induce coupled torsional vibrations. This type of misalignment was analyzed in works [6, 8–11], both in the case of assuming a direct, completely non-compliant joint of both coupling flanges and taking into account certain slight flexibility resulting from structural properties of screw connections and a possible presence of lamella discs. Since a magnitude of the coupling of torsional vibrations with bending vibrations caused by the parallel misalignment of shafts connected by such a coupling, as indicated in [8], is of the order of the square of the value of this misalignment δ_k^2, it can be considered negligible. Thus, the effect of coupling with torsional vibrations will not be taken into account here.

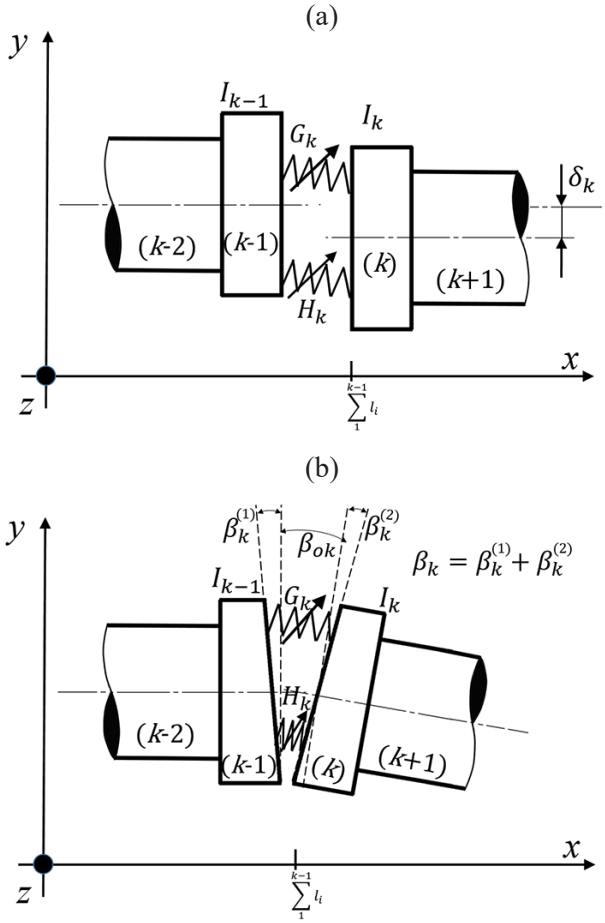

Fig. 2. The model of the coupling with an inner anisotropy and parallel (a) and angular (b) misalignment

The proposed mathematical model of the coupling characterized by the parallel misalignment comes down to a description of the connection of the extreme cross-section of the rotating Rayleigh or Timoshenko beam, representing in this model the k-1-st coupling flange, with the extreme cross-section of the analogous beam, representing the k-th flange, by means of a massless spring with the given shear stiffness G_{0k}, as shown in Fig. 2a. This description is a condition of equilibrium for viscoelastic, inertial and gyroscopic transverse forces, which in the case of applying the Rayleigh beam bending theory takes the following form:

$$
\begin{aligned}
&-EI_{k-1}\left(1+e\frac{\partial}{\partial t}\right)\frac{\partial^3 v_{k-1}(x,t)}{\partial x^3}+\rho I_{k-1}\frac{\partial^3 v_{k-1}(x,t)}{\partial x\partial t^2}-\\
&-2j\Omega(t)\rho I_{k-1}\frac{\partial^2 v_{k-1}(x,t)}{\partial x\,\partial t}-G_{0k}\cdot\Big(v_{k-1}(x,t)-\\
&-v_k(x,t)+D_k\Big(\Theta(t)-\Psi_k\Big)\Big)=0,\\
&EI_k\left(1+e\frac{\partial}{\partial t}\right)\frac{\partial^3 v_k(x,t)}{\partial x^3}-\rho I_k\frac{\partial^3 v_k(x,t)}{\partial x\partial t^2}+\\
&+2j\Omega(t)\rho I_k\frac{\partial^2 v_k(x,t)}{\partial x\,\partial t}+G_{0k}\cdot\Big(v_{k-1}(x,t)-\\
&-v_k(x,t)+D_k\Big(\Theta(t)-\Psi_k\Big)\Big)=0 \qquad \text{for } x=\sum_{i=1}^{k-1} l_i,
\end{aligned}
\tag{2}
$$

where: $D_k\big(\Theta(t)-\Psi_k\big)=\delta_k\Big[1-\cos\big(\Theta(t)-\Psi_k\big)\Big]+$
$+j\Big[-\delta_k\sin\big(\Theta(t)-\Psi_k\big)\Big]$,

$v_k(x,t)=u_k(x,t)+jw_k(x,t)$, $u_k(x,t)$ being the lateral displacement in the vertical direction and $w_k(x,t)$ the lateral displacement in the horizontal direction, both of the cross-section with the spatial coordinate x of the k-th beam segment, j denotes the imaginary number, $\Omega(t)$ is the current shaft rotational speed, $\Theta(t)$ is the current shaft rotation angle, e denotes the retardation time for beam flexural deformations, EI_k is the bending stiffness of the k-th beam segment with the geometric moment of inertia I_k and material density ρ, δ_k denotes the value of the parallel shaft misalignment, and Ψ_k is the phase angle of the coupling parallel misalignment.

In addition to the above-mentioned parallel misalignment, in a general case, angular misalignments may occur due to an improper mounting or imperfect machining of the coupling flanges. Then, the coupling faces can be not only mutually eccentric of the small off-set δ_k but also slightly deviated of the angle $\beta_k+\beta_{0k}$ from the plane perpendicular to the rotation axis, as shown in Fig. 2b, where angle β_k is a result of coupling flange machining error, and β_{0k} denotes the angular shaft misalignment, e.g. due to a misalignment of bearings.

In a structural physical model of the rotor machine drive system, the discussed type of coupling with the angular misalignment can also be represented by two flexible rotating beams corresponding respectively to both coupling flanges interconnected by a massless viscoelastic spring that substitutes flexural compliance of the assembly bolts and lamellar discs, as presented in Fig. 2b.

Here, the proposed mathematical model of the coupling characterized by the angular misalignment is reduced to a description of the connection of the extreme cross-section of the rotating Rayleigh or Timoshenko beam, representing in this model the k-1-st coupling flange, with the extreme cross-section of the analogous beam, representing the k-th flange, by means of a massless spring with the given bending stiffness H_{0k}, as shown in Fig. 2b. This description is a condition of equilibrium for viscoelastic and inertial bending moments, which in the case of applying the Rayleigh beam bending theory takes the following form:

$$\begin{aligned}
&EI_{k-1}\left(1+e\frac{\partial}{\partial t}\right)\frac{\partial^2 v_{k-1}(x,t)}{\partial x^2}+\\
&+H_{0k}\cdot\left(\frac{\partial v_{k-1}(x,t)}{\partial x}-\frac{\partial v_k(x,t)}{\partial x}-F_k\left(\Theta(t)-\Phi_k\right)\right)=0,\\
&EI_k\left(1+e\frac{\partial}{\partial t}\right)\frac{\partial^2 v_k(x,t)}{\partial x^2}+ \qquad \text{for } x=\sum_{i=1}^{k-1} l_i,\\
&+H_{0k}\cdot\left(\frac{\partial v_{k-1}(x,t)}{\partial x}-\frac{\partial v_k(x,t)}{\partial x}-F_k\left(\Theta(t)-\Phi_k\right)\right)=0,
\end{aligned} \tag{3}$$

where: $F_k\left(\Theta(t)-\Phi_k\right)=\left[\beta_{0k}-\beta_k\cos\left(\Theta(t)-\Phi_k\right)\right]+$
$+j\left[\beta_k\sin\left(\Theta(t)-\Phi_k\right)\right]$,

β_{0k} is the constant mutual angular misalignment of the k-1-th and k-th shaft segment axes, β_k denotes the angular misalignment due to a coupling flange machining error (see Fig. 2b), and Φ_k is the phase angle of the coupling angular misalignment.

2.3. Modelling of the coupling inner anisotropy

Based on reviews of the available literature, it can be concluded that the problem of anisotropy of the dynamic properties of rotor systems has not been thoroughly investigated so far. The main reasons for the occurrence of rotor shafts anisotropy were mainly different viscoelastic characteristics of bearing supports in the vertical and horizontal direction, as studied, e.g. in [12]. However, due to the legitimacy of maintaining a circular-symmetric shape of cross-sections of rotating elements, anisotropy of elastic or visco-inertial-elastic properties of the rotor shafts is observed relatively rarely, for example, in the case of rotors of two-pole generators or various types of atypical elements interconnecting rotor-shaft segments. This type of anisotropy is called the "inner anisotropy" of the rotor shaft. The inner anisotropy of rotor shafts, distributed continuously along their length, was investigated by means of the finite element method for cognitive purposes in the dissertation [13] and diagnosis of imperfections in [10]. Different values of shaft stiffness in mutually perpendicular directions to the axis of rotation due to a transverse crack in a given rotor shaft section can be considered the local anisotropy. Then, the resulting coupling of bending vibrations of the rotor shaft with its torsional vibrations can be used as a source of diagnostic information for detecting and identifying transverse cracks, which was the subject of research, e.g. in [14].

In the case of operation of couplings mutually connecting rotor shafts under high dynamic and static loadings, gradual degradation of the coupling components occurs, for example, in the form of loosening the connecting bolts or progressive plastic deformation of their seats or entire flanges' faces. As a result of such degradation, even with a correct assembly of the coupling, sometimes there is even a very significant difference in the bending stiffness of such a connection in two mutually perpendicular directions to the axis of rotation. So we are also dealing here with the inner anisotropy of the local type. This type of anisotropy due to the imperfection of the coupling components will be investigated here through a similar structural model as those that include the parallel and angular coupling misalignment. Its mathematical description is an analogous condition of equilibrium for viscoelastic, inertial and gyroscopic transverse forces and bending moments as the both above, which in the case of applying the Rayleigh beam bending theory takes the following form:

$$\begin{aligned}
&-EI_{k-1}\left(1+e\frac{\partial}{\partial t}\right)\frac{\partial^3 v_{k-1}(x,t)}{\partial x^3}+\rho I_{k-1}\frac{\partial^3 v_{k-1}(x,t)}{\partial x\partial t^2}-\\
&-2j\Omega(t)\rho I_{k-1}\frac{\partial^2 v_{k-1}(x,t)}{\partial x\,\partial t}-\\
&-\left(G_{0k}+G_{Vk}\,\mathrm{e}^{j\left(2\Theta(t)-\Delta_k\right)}\right)\cdot\left(v_{k-1}(x,t)-v_k(x,t)\right)=0,\\
&EI_k\left(1+e\frac{\partial}{\partial t}\right)\frac{\partial^3 v_k(x,t)}{\partial x^3}-\rho I_k\frac{\partial^3 v_k(x,t)}{\partial x\partial t^2}+\\
&+2j\Omega(t)\rho I_k\frac{\partial^2 v_k(x,t)}{\partial x\,\partial t}+\\
&+\left(G_{0k}+G_{Vk}\,\mathrm{e}^{j\left(2\Theta(t)-\Delta_k\right)}\right)\cdot\left(v_{k-1}(x,t)-v_k(x,t)\right)=0,\\
&EI_{k-1}\left(1+e\frac{\partial}{\partial t}\right)\frac{\partial^2 v_{k-1}(x,t)}{\partial x^2}+\\
&+\left(H_{0k}+H_{Vk}\,\mathrm{e}^{j\left(2\Theta(t)-\Delta_k\right)}\right)\cdot\left(\frac{\partial v_{k-1}(x,t)}{\partial x}-\frac{\partial v_k(x,t)}{\partial x}\right)=0,\\
&EI_k\left(1+e\frac{\partial}{\partial t}\right)\frac{\partial^2 v_k(x,t)}{\partial x^2}+ \qquad \text{for } x=\sum_{i=1}^{k-1} l_i,\\
&+\left(H_{0k}+H_{Vk}\,\mathrm{e}^{j\left(2\Theta(t)-\Delta_k\right)}\right)\cdot\left(\frac{\partial v_{k-1}(x,t)}{\partial x}-\frac{\partial v_k(x,t)}{\partial x}\right)=0,
\end{aligned} \tag{4}$$

where: $G_{0k} = \frac{1}{2}\left(G_\eta + G_\varsigma\right)$, $G_{Vk} = \frac{\sqrt{2}}{2}\left(G_\eta + G_\varsigma\right)$,

$H_{0k} = \frac{1}{2}\left(H_\eta + H_\varsigma\right)$, $H_{Vk} = \frac{\sqrt{2}}{2}\left(H_\eta + H_\varsigma\right)$,

G_η, G_ζ and H_η, H_ζ are respectively the shear and bending stiffness of the massless spring connecting both coupling flanges about two mutually perpendicular axes η and ζ of the coordinate system rotating with the shaft, see Fig. 1, and Δ_k is the phase angle of the coupling inner anisotropy.

2.4. Mathematical modelling of the coupling with combined imperfections.

A proper combination of relationships (2)–(4) leads to the complete mathematical model of the coupling characterized by the simultaneous parallel and angular misalignment and the inner anisotropy. Then, one obtains the resultant conditions of equilibrium for viscoelastic, inertial and gyroscopic transverse forces and bending moments:

$$
\begin{aligned}
&-EI_{k-1}\left(1+e\frac{\partial}{\partial t}\right)\frac{\partial^3 v_{k-1}(x,t)}{\partial x^3}+\rho I_{k-1}\frac{\partial^3 v_{k-1}(x,t)}{\partial x\partial t^2}-\\
&-2j\Omega(t)\rho I_{k-1}\frac{\partial^2 v_{k-1}(x,t)}{\partial x\,\partial t}-\left(G_{0k}+G_{Vk}\,\mathrm{e}^{j\left(2\Theta(t)-\Delta_k\right)}\right)\cdot\\
&\cdot\left(v_{k-1}(x,t)-v_k(x,t)+D_k\left(\Theta(t)-\Psi_k\right)\right)=0,\\
&EI_k\left(1+e\frac{\partial}{\partial t}\right)\frac{\partial^3 v_k(x,t)}{\partial x^3}-\rho I_k\frac{\partial^3 v_k(x,t)}{\partial x\partial t^2}+\\
&+2j\Omega(t)\rho I_k\frac{\partial^2 v_k(x,t)}{\partial x\,\partial t}+\left(G_{0k}+G_{Vk}\,\mathrm{e}^{j\left(2\Theta(t)-\Delta_k\right)}\right)\cdot\\
&\cdot\left(v_{k-1}(x,t)-v_k(x,t)+D_k\left(\Theta(t)-\Psi_k\right)\right)=0,\\
&EI_{k-1}\left(1+e\frac{\partial}{\partial t}\right)\frac{\partial^2 v_{k-1}(x,t)}{\partial x^2}+\left(H_{0k}+H_{Vk}\,\mathrm{e}^{j\left(2\Theta(t)-\Delta_k\right)}\right)\cdot\\
&\cdot\left(\frac{\partial v_{k-1}(x,t)}{\partial x}-\frac{\partial v_k(x,t)}{\partial x}-F_k\left(\Theta(t)-\Phi_k\right)\right)=0,\\
&EI_k\left(1+e\frac{\partial}{\partial t}\right)\frac{\partial^2 v_k(x,t)}{\partial x^2}+\left(H_{0k}+H_{Vk}\,\mathrm{e}^{j\left(2\Theta(t)-\Delta_k\right)}\right)\cdot\\
&\cdot\left(\frac{\partial v_{k-1}(x,t)}{\partial x}-\frac{\partial v_k(x,t)}{\partial x}-F_k\left(\Theta(t)-\Phi_k\right)\right)=0\quad\text{for } x=\sum_{i=1}^{k-1}l_i.
\end{aligned}
\tag{5}
$$

Here, the all symbols above have been already defined for relationships (2)–(4), and the explicit time functions of the shaft current rotation angle $\Theta(t)$, which occur in (5), i.e., $D_k\left(\Theta(t)-\Psi_k\right)$, $F_k\left(\Theta(t)-\Phi_k\right)$ and $C\cdot\exp\left(j\left(2\Theta(t)-\Delta_k\right)\right)$, where $C = G_{Vk}$ or H_{Vk}, can be treated as concentrated external excitations applied to both flanges of the coupling.

3. MODELLING OF THE ENTIRE ROTOR-SHAFT SYSTEM

In order to obtain sufficiently reliable results of qualitative analyses and numerical simulations for the rotor-shaft system, all computations will be performed by means of the hybrid structural modelling approach, which uses flexurally deformable, as in [14–16], and torsionally deformable, as in [15, 17], continuous viscoelastic beam finite elements combined with discrete oscillators. Identically, as in the case of a classical discretized beam finite element formulation, the following points are considered when using such modelling: the rotor-shaft geometry, its material properties, gyroscopic effects and shaft material damping as described by the three-parameter solid model. Here, in the hybrid model, successive cylindrical segments of the stepped rotor-shaft are represented by flexurally deformable cylindrical finite elements with continuously distributed inertial-visco-elastic properties. However, some heavy rotors, dynamic deformations of which are negligible, can be substituted by rigid bodies attached to the continuous finite element extreme cross-sections.

Each journal bearing is represented by a dynamic oscillator of two degrees of freedom, using which, in addition to the oil-film interaction, the viscoelastic properties of the bearing housing and foundation are included. By means of this bearing model, it is possible to represent reliably kinetostatic and dynamic anisotropic and anti-symmetric properties of the oil film in the form of a variable or constant damping and stiffness coefficients. The mutual combination of continuous finite elements together with discrete oscillators and rigid bodies according to the structure of the real object results in a hybrid mechanical model created in this way. Figure 3 presents the real object

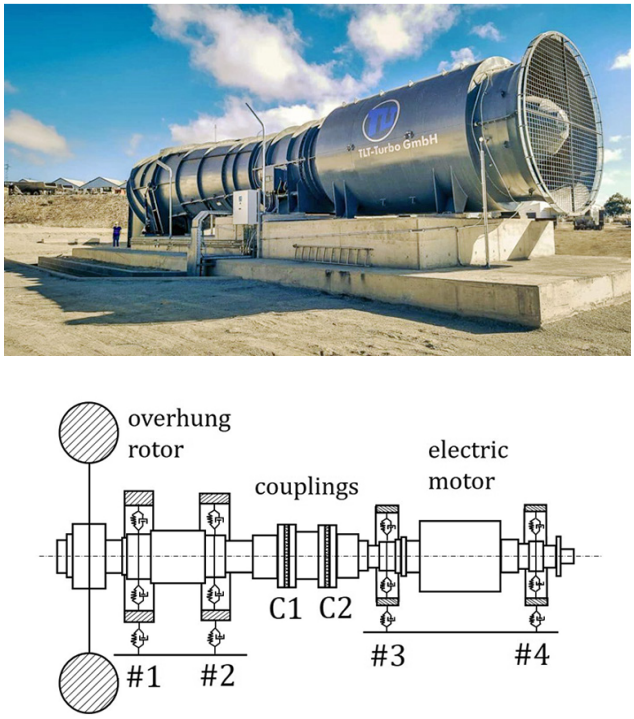

Fig. 3. The industrial blower with an overhung rotor: the real object and its hybrid mechanical model

and the hybrid model of that representative rotor-machine with an overhung rotor and driven by an electric motor by means of two rigid couplings.

4. MATHEMATICAL SOLUTION OF THE PROBLEM

The complete mathematical formulation and solution for the rotor-shaft system hybrid model applied here can be found, e.g. in [14–16]. In this model, the flexural motion of cross-sections of each viscoelastic continuous finite element is governed by the partial differential equations derived using the Rayleigh or Timoshenko rotating-beam theory. In such equations, there are contained gyroscopic forces mutually coupling rotor-shaft bending vibrations in the horizontal and vertical plane. The analogous coupling effect caused by the system rotational speed-dependent shaft material damping, described by the use of the three-parameter solid model, is also included.

As in the works [14–16], mutual connections of the successive macro-elements creating the stepped shaft and their interactions with the bearing supports and rigid bodies representing the heavy rotors are described by equations of compliance conditions. These are the equations of geometrical conditions of equality for translational and rotational displacements of extreme cross-sections of the continuous finite elements. The second group of compliance conditions are dynamic ones, which generally contain linear, parametric and nonlinear equations of equilibrium for concentrated external forces, static and dynamic unbalance forces and moments, inertial, elastic and external damping forces, support reactions and gyroscopic moments. Interaction of the shaft with discrete oscillators representing the bearing supports is also described by means of the dynamic compliance conditions. Such compliance conditions contain anti-symmetrical terms with cross-coupling oil-film stiffness and damping components, which couple shaft bending vibrations in two mutually perpendicular planes. In these equations, the damping and stiffness coefficients can be variable or constant when the nonlinear properties of the oil film are not taken into consideration. Dynamic properties of the coupling model with imperfections are also described by the dynamic compliance conditions (5) containing concentrated harmonic excitations oscillating with a single- 1X and double-synchronous 2X frequency.

The solution for simulations of the forced lateral vibrations has been obtained using the analytical–computational approach described in detail in [14, 15]. In the first step, the set of bending eigenmode functions is determined by solving the differential eigenvalue problem for the linear orthogonal system. Next, all anti-symmetric, gyroscopic and parametric terms omitted to solve the eigenvalue problem are regarded here as response-dependent external excitations. Finally, for the hybrid model of the rotor-shaft system, the Fourier solution in the form of series in the orthogonal eigenfunctions is applied, which leads to an infinite number of known separate ordinary differential equations in modal coordinates. However, the above-mentioned response-dependent external excitations and gyroscopic forces mutually couple these equations in the case considered here. Thus, consequently, one obtains the following set of parametric ordinary differential equations in the modal coordinates:

$$\mathbf{M}_0\ddot{\mathbf{r}}(t)+\mathbf{D}(\Omega)\dot{\mathbf{r}}(t)+ \\ +\left[\mathbf{K}(\Omega)+\mathbf{K}_a\left(\exp(j2\Theta(t))\right)\right]\mathbf{r}(t)=\mathbf{F}(\Omega^2,\Theta(t)), \tag{6}$$

where: $\mathbf{D}(\Omega)=\mathbf{D}_0+\mathbf{D}_g(\Omega)$ and $\mathbf{K}(\Omega)=\mathbf{K}_0+\mathbf{K}_b+\mathbf{K}_d(\Omega)$, $\Theta(t)=\int_0^t\Omega(\tau)d\tau$.

The symbols $\mathbf{M}_0$, $\mathbf{K}_0$ are the diagonal modal mass and stiffness matrices, respectively, $\mathbf{K}_a$ is the symmetrical matrix of parametric excitation with a double-synchronous frequency 2X due to anisotropic properties of the coupling, $\mathbf{D}_0$ denotes the symmetrical damping matrix, and $\mathbf{D}_g(\Omega)$ is the skew-symmetrical matrix of gyroscopic effects. Skew- or non-symmetrical elastic properties of the bearings are expressed by matrix $\mathbf{K}_b(\Omega)$. Anti-symmetrical effects due to the three-parameter solid material damping model of the rotating shaft are described by the skew-symmetrical matrix $\mathbf{K}_d(\Omega)$, symbol $\mathbf{F}\left(\Omega^2(t),\Theta(t)\right)$ denotes the vector of external excitations caused by static and dynamic unbalances, gravitational forces, and parallel and angular misalignments of the rotor shaft sections. Here, the unbalance terms depending on rotor-shaft angular acceleration and velocity are negligible. The modal coordinate vector $\mathbf{r}(t)$ consists of the unknown time functions standing in the Fourier solution. The mathematically proven quick convergence of the Fourier solution allows for a limitation of the number of equations (6) to solve to the number of bending eigenmodes taken into consideration in the frequency range of interest. In order to determine eigenvalues of the rotor-shaft dynamic model, it is convenient to transform its modal motion equations (6) to analogous equations in the modal state coordinates, as described in the paper [16]. Consequently, it is possible to solve the standard eigenvalue problem in which a characteristic non-symmetrical matrix is reduced to the Hessenberg form by means of the Hausholder transformation. Then, the final determination of the eigenvalue real and imaginary parts for each bending eigenmode of the system under study is achieved by means of the commonly known QR algorithm.

5. COMPUTATIONAL RESULTS

The object of computations is a heavy industrial blower driven by an asynchronous motor with a power of 6.3 MW at the rated speed of 993 rpm via two lamella couplings C1 and C2, interconnected by an intermediate shaft, as schematically shown in Fig. 3. The rotor of this blower is characterized by an outer diameter of 4.4 m and a total mass 5.61 times greater than the mass of its shaft. This shaft is suspended on two oil-journal bearings mutually distant by 0.79 m. The span of the rolling element bearings supporting the motor rotor is equal to 2.345 m. In the hybrid model, subsequent cylindrical sections of the real rotor-shaft of this device have been substituted by 42 continuous beam finite elements.

The model update was carried out in four stages. In the first one, geometric dimensions and material constants of individual beam finite elements were established based on the technical documentation of the real object. On this basis, stiffness and damping coefficients of the bearings and their housing were calculated too. However, all imperfection parameters, i.e., the rotor unbalances, parallel and angular misalignments of both couplings and coupling inner anisotropy factors, each of which is usually difficult to identify, must have been initially approximated by means of experimental measurements performed using the real object. Thus, in the second stage, basing on the fundamental synchronous components 1X of the measured system responses, the unbalances of the overhung blower rotor, and the driving motor rotor and coupling parallel misalignments have been estimated by means of the automated trial-and-error approach. Since the measured responses were also characterized by the double- 2X and triple-synchronous 3X components, the most probably induced by the internal anisotropy of the couplings, in the third stage of model updating the coupling inner anisotropy factors defined as $\kappa_k = G_{Vk}/G_{0k}$ and $\chi_k = H_{Vk}/H_{0k}$, $k = 1, 2$, had to be determined in the same way. In order to achieve the greatest possible similarity of the measured and computed responses in the vertical and horizontal direction, the initially calculated values of the stiffness and damping coefficients of all four bearing housings had to be subjected to additional fine-tuning in the fourth stage. Finally, the best mutual similarity of the measured and computed results have been obtained for the blower rotor static unbalance admissible eccentricity $\varepsilon = 0.081$ mm, its dynamic unbalance angular inclination $\alpha = 0.05$ deg, the parallel misalignments of both couplings $\delta_{1,2} = 0.5$ mm, coupling inner anisotropy factors $\kappa_k = G_{Vk}/G_{0k}$ and $\chi_k = H_{Vk}/H_{0k}$, $k = 1, 2$, both equal to 0.2, and for the motor rotor uniform mass admissible eccentricity $\nu = 0.082$ mm. In all computational tests, the retardation time e of the structural damping corresponded to the loss-factor of 0.0094 and the logarithmic decrement of the rotor-shaft free lateral vibrations equal to 0.0296, which take into consideration material losses and frictional effects in the couplings. In Fig. 4 there are presented measured and calculated time-histories of the horizontal vibration velocities registered at the constant rotational speed for the bearing support #1 at the blower rotor and bearing #3 at the asynchronous motor.

Despite the most careful tuning of the tested machine model, the exact identification of the values characterizing the imperfections in question is extremely difficult. Therefore, in the further part of this work, these parameters will be treated as so-called uncertain and will receive special attention.

5.1. Stability analysis of the blower rotor-shaft-bearing system

In the form of determining the rotor-shaft system's eigenvalue real parts, a stability analysis has been performed for parameters of the experimentally tuned blower rotor-shaft system model with coupling inner anisotropy neglected and in the frequency range comprising the first four bending eigenmodes. Figure 5 illustrates the characteristics of these eigenvalue real parts obtained in the rotational speed range of 0–2400 rpm, corresponding to 0–40 rev/s. For greater clarity, the respective successive eigenfunctions are also depicted on the left-hand side of the diagram. From the plots illustrated in this figure, it is evident that not all eigenvalue real parts are negative, which means that the blower rotor-shaft system under study possesses a degree of instability. Namely, above the rated speed of 993 rpm, i.e., at 30 rev/s (1800 rpm), the first eigenmode begins to be unstable.

In order to perform analogous stability analysis for the parametric system, i.e., taking into account the inner anisotropy of the couplings, the harmonic balance method was used. For this purpose, the first five eigenmodes of the object under study have been considered in the frequency range of 0–60 Hz. The results of standard computations obtained by means of this approach indicated three classic zones of instability in the form of periodic parametric resonances of the first order in the vicinity of the first three system natural frequencies, i.e., between ~9–16, 20–25 and 29–36 Hz. This fact has been confirmed by simulations of the blower start-up from a standstill to nominal operation within 90 s carried out for three inner anisotropy factors G_{Vk}/G_{0k} and H_{Vk}/H_{0k}, $k = 1, 2$, equal to 0.2, 0.3 and 0.4. In Fig. 6, in time and frequency domain, there are presented

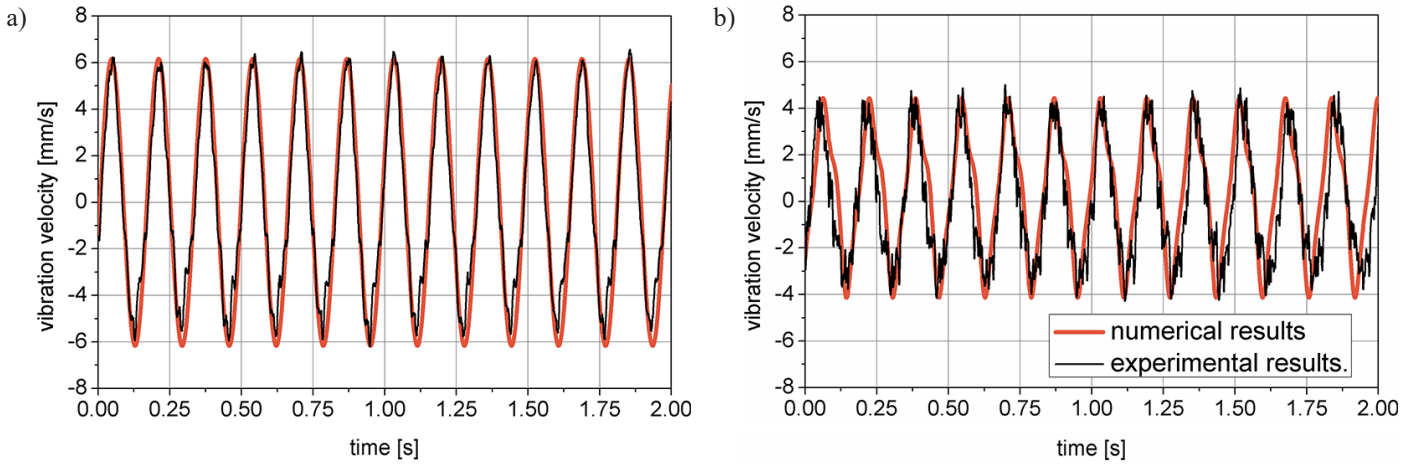

Fig. 4. Measured and calculated vibration velocities at housings of bearing #1 (a) and bearing #3 (b)

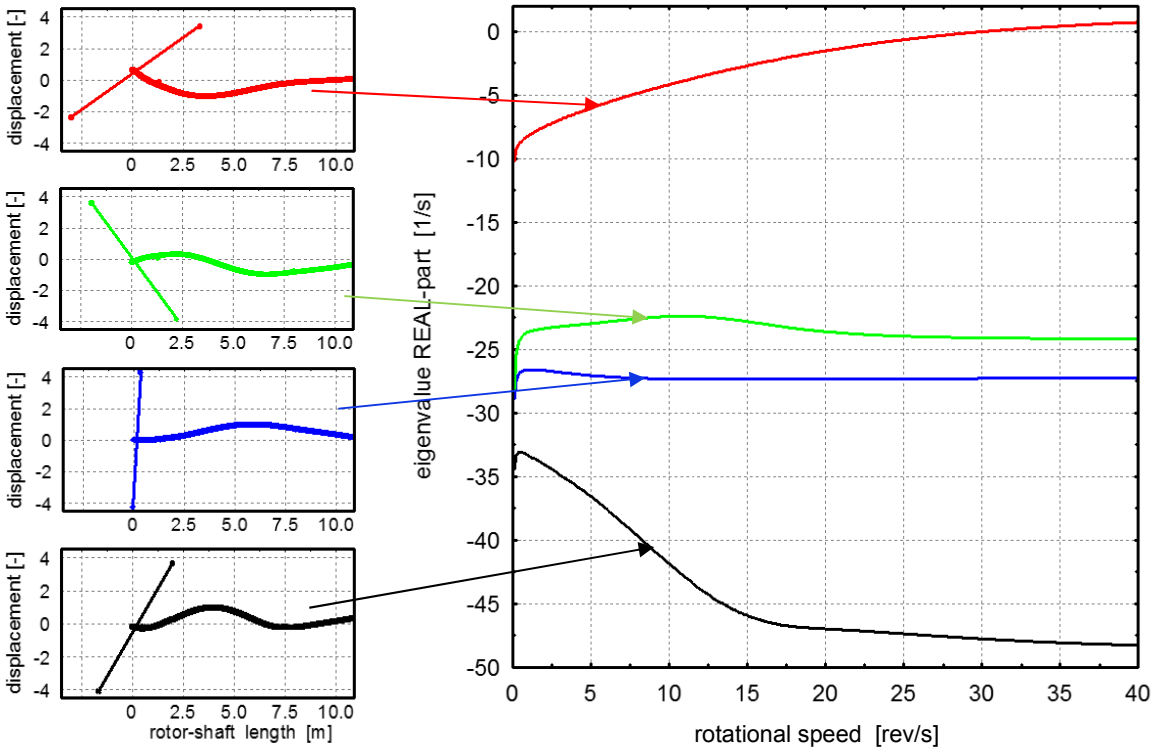

Fig. 5. Maximal eigenvalue real parts of the blower rotor-shaft system

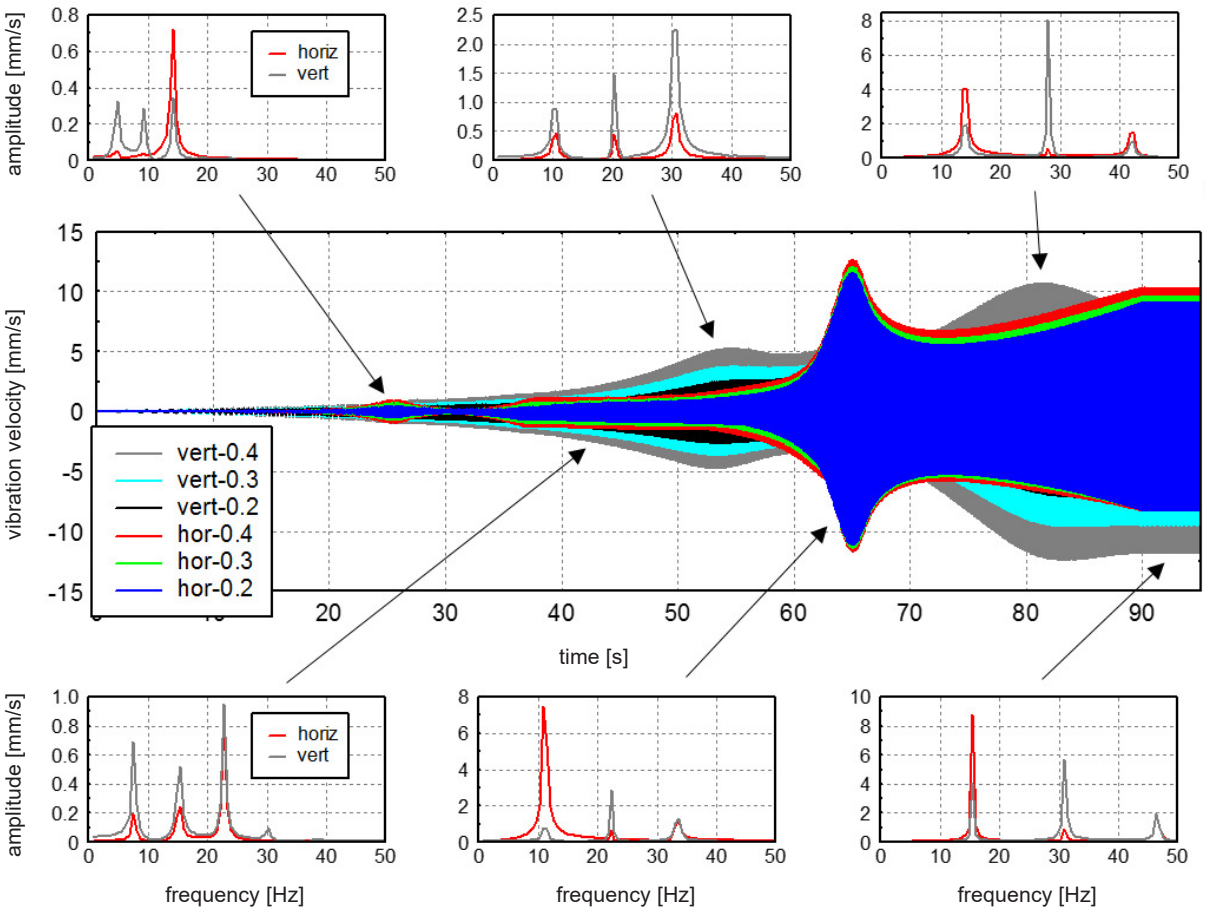

Fig. 6. Transient and steady-state parametric response of the blower rotor-shaft system

plots of the vertical and horizontal vibration velocity registered for the housing of bearing #3, which is close to the second rigid coupling C2, see Fig. 3. Namely, during the start-ups, between the 23rd and 28th second, the first parametric amplification of the first instability zone is observed. Next, after the 35th second also the second zone is activated, and after the 50th second, all three instability zones have been significantly amplified. Successively, in the horizontal direction at the ca. 65th second of the run-up, severe peaks of an ordinary resonance with the system first eigenmode occur, while due to both couplings' inner anisotropy also the second and third parametric instability zones are remarkably excited.

Because of a strong anisotropy of the bearing supports, the next peaks of the transient responses are observed in the vertical plane due to the periodic parametric resonance with the system second eigenmode. Then, in steady-state operational conditions, i.e., after the 90th second, the synchronous excitation frequency 1X of 16.55 Hz is predominant. However, since its double value 2X, equal to 33.1 Hz, coincides with the third parametric instability zone, this results in the additional severe vibration component. From the time-histories of the blower, lateral oscillation velocities demonstrated in Fig. 6; one can remark that a contribution of the parametric effects to the system transient and steady-state dynamic responses seems to be proportional to the factors G_{Vk}/G_{0k} and H_{Vk}/H_{0k}, $k = 1, 2$, of the inner anisotropy of the rigid couplings C1 and C2 connecting the blower with the asynchronous motor.

5.2. Testing of the blower rotor-shaft system sensitivity to excitations caused by imperfections.

Assuming all modal harmonic excitations contained in the right-hand side vector $\mathbf{F}(\Omega^2, t)$ of Equations (6) fluctuate mutually in phase, amplitudes of successive components of this vector can be expressed as:

$$\bar{F}_i(\varepsilon,\alpha,\delta_1,\beta_1,\delta_2,\beta_2,\nu) = \Omega^2 m_R V_{Ri}\varepsilon + \Omega^2 (I_\xi - I_\eta)\Phi_{Ri}\alpha + \\ + E_{01}\Delta V_{C1i}\delta_1 + F_{01}\Delta V'_{C1i}\beta_1 + E_{02}\Delta V_{C2i}\delta_2 + F_{02}\Delta V'_{C2i}\beta_2 + \\ + \Omega^2 \rho_M A_M \left(\int_0^{l_M} V_{Mi}(x)\cdot \mathrm{d}x \right)\cdot \nu, \quad i = 1, 2, \ldots \tag{7}$$

where m_R, V_{Ri}, Φ_{Ri} are respectively the mass, normalized eigen-displacement and eigen-inclination angle of the overhung rotor, ΔV_{Cki}, $\Delta V'_{Cki}$ denote differences of coupling flange eigen-displacements and eigen-inclination angles, $k = 1, 2$, ρ_M, A_M, l_M, are respectively the average density, cross-section area and length of the electric motor rotor, $V_{Mi}(x)$ is the eigen-displacement function of this rotor, and ν denotes the uniformly distributed mass eccentricity along with the motor rotor, which causes its static unbalance. These amplitudes are sums of linear functions of the rotor-shaft imperfection parameters ε, α, δ_1, β_1, δ_2, β_2, ν treated here as uncertain parameters of the system under study. Their multipliers in (7), being functions of system structural parameters, modal displacements and the nominal rotational speed value Ω, can be interpreted as external excitation gains for successive eigenmodes, which serve as a measure of system sensitivity to induction of forced lateral vibrations. For the hybrid model of the industrial blower rotor-shaft system under consideration, these gains have been illustrated in Fig. 7 in the form of a block diagram. In this figure, the blocks corresponding to the individual system imperfections are marked by the following colours: red – the static unbalance of the rotor (RSU), navy blue – rotor dynamic unbalance (RDU), green – parallel misalignment of coupling C1 (C1PM), violet – angular misalignment of coupling C1 (C1AM), grey – parallel misalignment of coupling C2 (C2PM), blue – angular misalignment of coupling C2 (C2AM) and brown – static unbalance of the motor rotor (MSU). It should be noted that these excitation gains have different physical dimensions, i.e., N/m and N, and therefore not all of them can be directly compared. Nevertheless, their absolute values are increase gradients of magnitudes of the given types of excitations, being the components of successive elements of vector $\mathbf{F}(\Omega^2, t)$. Thanks to this, their numerical values can be treated as a sensitivity measure of the vibrating system to oscillations caused by the types of imperfections under consideration. Based on the heights of individual blocks presented in Fig. 7, it can be concluded that the first fundamental eigenmodes of this system are the most sensitive to excitations due to static and dynamic unbalances. Although the numerical values of the gains for the excitations caused by the dynamic unbalances are often respectively slightly smaller than these due to the static ones, but it should be remembered that in practice, the angular deviations can be great enough to make the dynamic unbalance of the overhung rotors much more dangerous than the static imbalances which are usually limited by strict industrial standards. However, an influence of coupling parallel and angular misalignments is quite remarkable for the fundamental eigen-

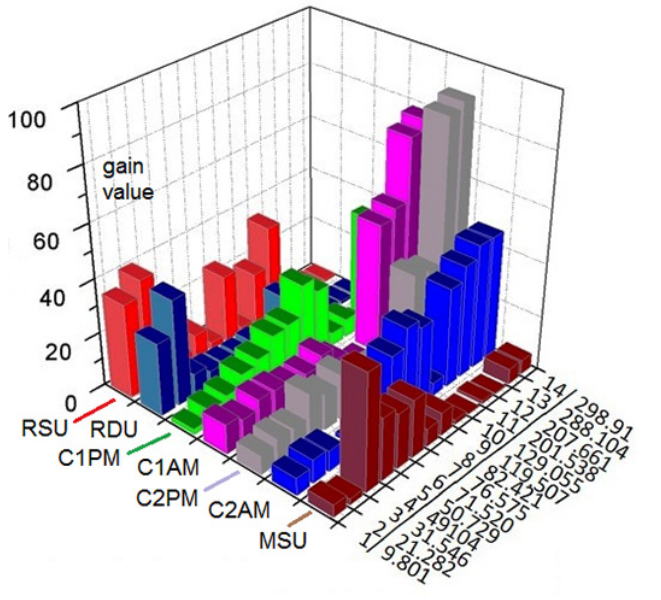

Fig. 7. External excitation gains for successive eigenmodes of the blower rotor-shaft system

modes but particularly significant for excitations with higher frequencies, i.e., above 70 Hz and more.

5.3. An analysis of dynamic responses caused by the imperfections of the rotor-shaft system

Since all kinds of imperfections of the rotor machine with the overhung rotor under study are treated here as uncertain parameters, their influence on the system's dynamic behaviour can be investigated by means of a stochastic or interval approach. Generally, uncertainty analyses in engineering can be performed in two ways, i.e., using the polynomial chaos expansion method in the random approach, as in [10, 18], and using the interval method described, e.g., in [19, 20]. The random uncertainties are used to describe those whose exact probability density functions (PDFs) are already known. Then, the PDFs of a given random quantity can be constructed basing on sufficient statistical information when there are multiple samples or validated empirical distribution models. Only under this condition they are precise and accurate in uncertainty propagation analysis, and using the polynomial chaos expansion method, reliable results in stochastic modelling of the random variables and processes can be obtained. For example, to assume proper PDFs applied for crack detection and identification in [14], fracture mechanics fundamentals were used.

Similarly, in [18], the PDF was estimated basing on deep knowledge about visco-elastic properties of the journal bearings and manufacturing technology of the rotor-machine, in the structural model of which bearing stiffness and damping coefficients, as well as rotor mass eccentricities, were treated as uncertain parameters. Therefore, the PDF is recently popular and widely applied in analyses of the uncertainty of mechanical systems and has also been successfully adapted as an effective method for stochastic dynamic investigations of rotor machines [10]. Nevertheless, it is necessary to be conscious that insufficient prior knowledge of uncertain structural parameters, or their changing with time due to operational degradation of the most heavily affected machine components, make results obtained using the random approach unrealistic.

Interval variables of the uncertain parameters characterized only by their bounds can alternatively and successfully be applied in situations where exact PDFs of uncertain parameters are unavailable. As indicated in [20], calculation results obtained by means of the interval approach, when the parameter perturbation method is applied, are consistent with the theoretical proofs, which justify that the dynamic interval responses enclose those determined using the probabilistic approach. This means that the lower bounds determined by the parameter perturbation method are smaller than those predicted by the probabilistic approach. The upper bounds calculated using the parameter perturbation method are greater than those obtained by the use of the probabilistic approach. In addition to good robustness to uncertainty, this property of the obtained results can be considered safer from the viewpoint of engineering practice, which makes the interval method very suitable in analyzing dynamic responses of the rotor-shaft systems, e.g. in [19]. For this reason, in [21], to use advantages of both approaches mutually confronted above, for engineering problems with partial, incomplete information, the random and interval uncertainties are simultaneously included in the form of a standard algorithm, called hybrid uncertainties.

Distributions of the uncertain parameters of the industrial blower being tested are rather unknown. However, their intervals can be got easier. Then, an interval analysis can be used most conveniently when such information about these uncertain variables in the form of a preference or probability function is not available. Thus, similarly as in [19,20], the interval uncertainty approach has been applied here, in which the imperfection parameters $\mu = \varepsilon,\ \alpha,\ \delta_1,\ \beta_1,\ \kappa_1,\ \chi_1,\ \delta_2,\ \beta_2,\ \kappa_2,\ \chi_2,\ \nu$ are uncertain but bounded. They all can be described by interval notation as $\mu = [\mu^C - \sigma\mu^C,\ \mu^C + \sigma\mu^C]$, where μ^C denotes their nominal values and σ is the deviation coefficient.

First, this section will carry out a qualitative analysis of the object's sensitivity under consideration to excitations caused by the aforementioned imperfections in the form of interval frequency response characteristics determined in steady-state operational conditions at the constant rotational speed of 993 rpm. In the discussed case, the sources of excitations, according to the models of these imperfections described by equations (1)–(5) and (7), are transverse forces ("forc") and bending moments ("mom") applied in places of the rotor-shaft model corresponding to the position of the blower rotor ("rotor"), both C1 and C2 couplings and the rotor of the electric motor ("motor"). In this way, in a frequency range of interest, it is possible to investigate the sensitivity of the system being tested to excitations caused by the dynamic unbalance of the blower rotor, parallel and angular misalignments of both couplings and their internal anisotropy, as well as static, unbalances of the blower rotor and electric motor rotor. For the imperfections under consideration in the excitation frequency range of 0–300 Hz with the maximum expected in practice deviation coefficient $\sigma = 0.15$ in Fig. 8, there are presented the interval frequency response characteristics determined for horizontal displacements at the housings of bearing #1 in the vicinity of the blower overhung rotor (Fig. 8a) and bearings #3 and #4 which support the motor rotor (Fig. 8b, 8c). All plots in these figures are characterized by the local maxima corresponding to the successive system natural frequencies listed in Fig. 7. It is worth noting that an influence of the excitation corresponding to the blower rotor dynamic unbalance is greater than that of its static unbalance and is predominant at frequencies smaller than 80 Hz at the housings of bearing #1 (Fig. 8a) and #3 (Fig. 8b), contrary to the excitation corresponding to the static unbalance of the motor rotor, which is the most significant at the housing of bearing #4 (Fig. 8c). However, an influence of excitations corresponding to coupling imperfections begins to dominate over those of unbalances at excitation frequencies bigger than 125 Hz at the housings of bearing #3 and #4, as shown in Figs. 8b and 8c. Nevertheless, at greater oscillation frequencies, a relatively high level of damping, taken into account in determining the frequency response characteristics, significantly reduces the amplitudes of rotor-shaft lateral vibrations excited by imperfections of both couplings to significant but not dominant values.

Then, a quantitative analysis of the influence of the imperfections will be carried out with their parameters established

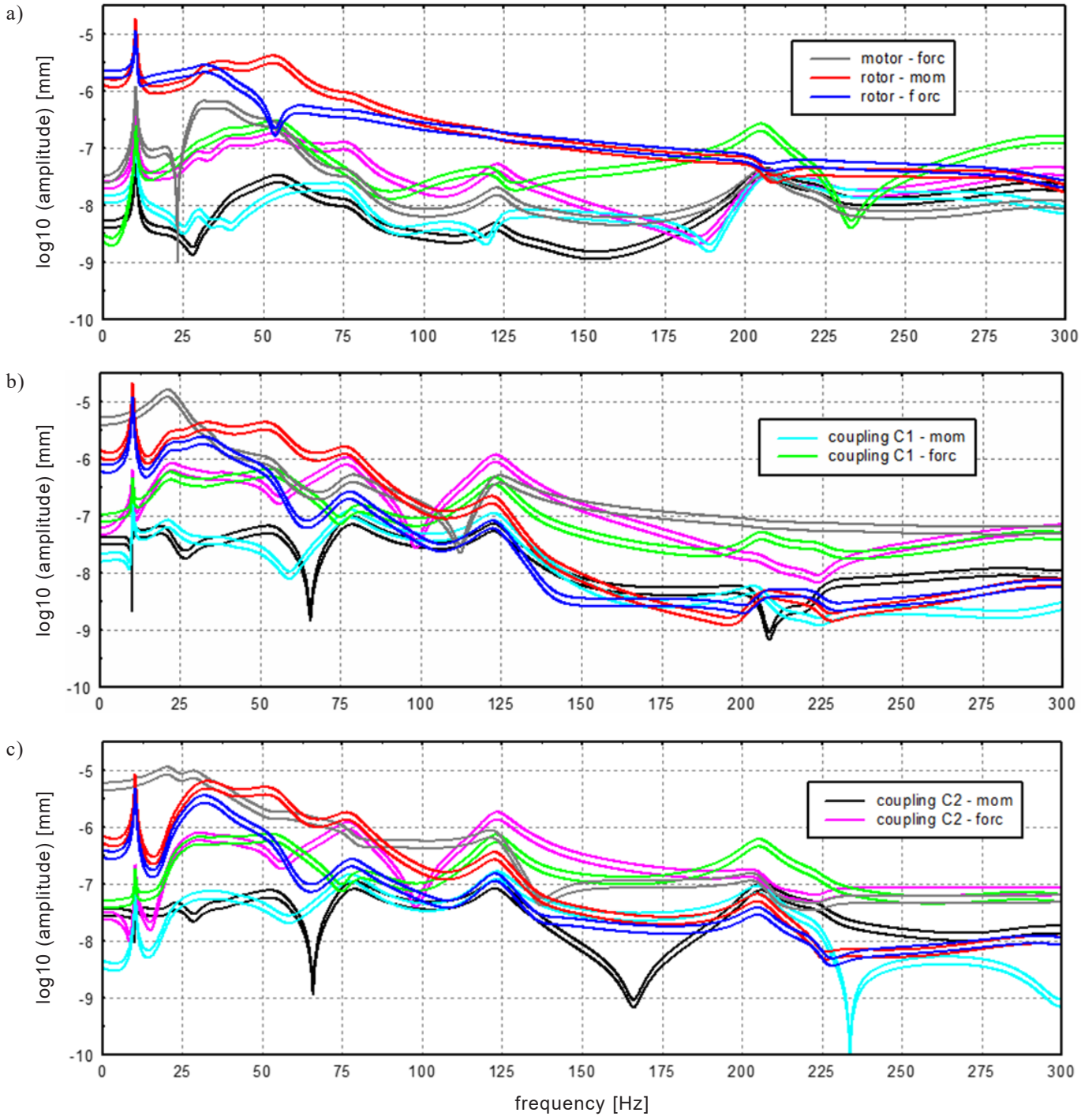

Fig. 8. Interval frequency response characteristics at housings of bearing #1 (a), #3 (b) and #4 (c) induced by system imperfections

experimentally during the tuning of the hybrid model of the industrial blower under consideration. Here, as listed at the beginning of this chapter, $\varepsilon^{C} = 8.1 \cdot 10^{-5}$ m, $\alpha^{C} = 0.05$ deg, $\delta_1^{C} = \delta_2^{C} = 0.5 \cdot 10^{-4}$ m, $\kappa_1^{C} = \chi_1^{C} = \kappa_2^{C} = \chi_2^{C} = 0.2$ and $\nu^{C} = 8.2 \cdot 10^{-5}$ m. The angular misalignments of both couplings C1 and C2 described by parameters β_k and β_{0k} were not considered because, as shown by the measurement results recorded on the aforementioned real object, their influence on dynamic excitations turned out to be negligible.

Individual contributions of the listed imperfections under study as well as their resultant influence on dynamic responses of the blower rotor-shaft system will be investigated in steady-state operating conditions at the nominal rotational speed of 993 rpm and for the same deviation coefficient $\sigma = 0.15$, as above. Figure 9 presents time-histories of the vertical vibration velocity registered at the housing of bearing #1 (Fig. 9a) and at the housings of bearings #3 and #4 (Figs. 9b, 9c). These figures show plotted time-histories of the system responses obtained

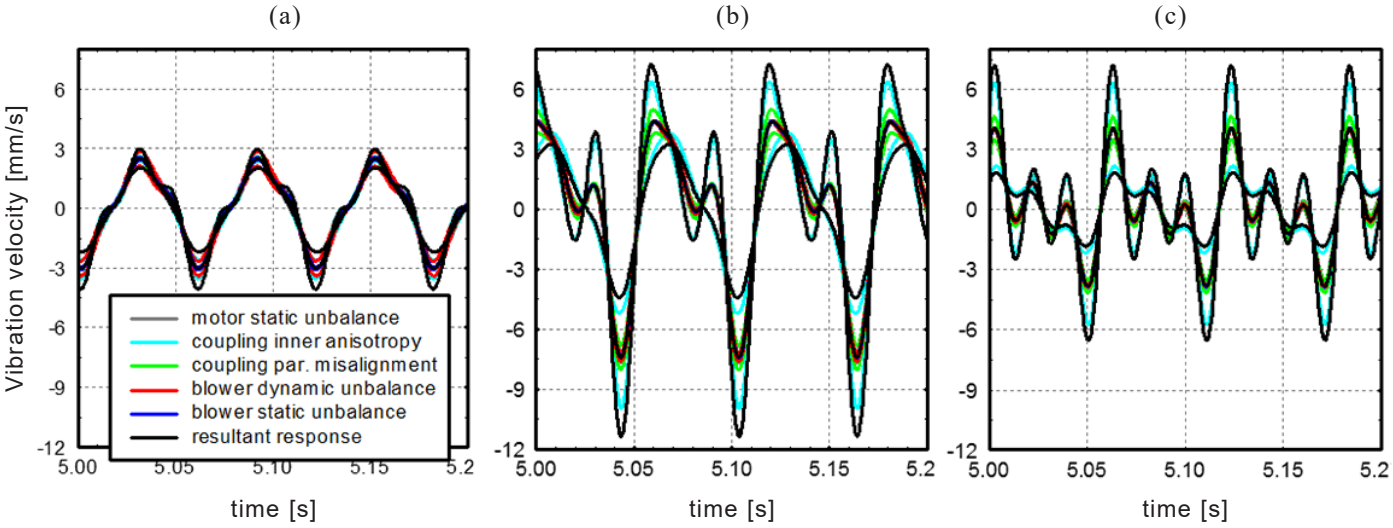

Fig. 9. Vibration velocity fluctuations at housings of bearing #1 (a), #3 (b) and #4 (c) induced by system imperfections

for the lower and upper bounds of the intervals of individual imperfections with the remaining nominal imperfection parameters and the resultant time-histories following from the lower and upper bounds of the intervals of all tested uncertain parameters together.

From the plots presented in these figures, it follows that the blower rotor-shaft system is more sensitive to the dynamic unbalance of the overhung rotor than to the static one, particularly close to its location at bearing #1. The parallel misalignments of couplings C1 and C2 are felt more strongly at the housings of bearings #3 and #4, as shown in Figs. 9b and 9c, which seems to be rather intuitive. However, a quite strong influence of the coupling inner anisotropy is remarkable at all three bearing housings. Nevertheless, the most significant is the severity of the system dynamic responses observed at the housing of bearing #3, which is closest to both couplings C1 and C2. Namely, these responses are characterized by great extreme values, and here, the contributions of all individual system imperfections are very clear. This effect results from the dynamic properties of the entire blower drive system, which are expressed, among others, by lateral displacement distributions of the fundamental eigenforms shown in Fig. 5. Moreover, it is worth noting that this fact can be particularly essential from the viewpoint of a planned installation of monitoring and diagnostic devices on the real object under consideration.

6. FINAL REMARKS

In the paper, a stability and sensitivity analysis has been performed for the rotating machine with an overhung rotor through a hybrid model, in which typical imperfections of such an object were included. The results of qualitative studies and numerical simulations performed for this system showed that even very small mounting inaccuracies of its heavy overhung rotor, which cause a dynamic unbalance, lead to much more severe lateral vibrations than analogous oscillations induced by an admissible static imbalance. Furthermore, the assembly faults of rigid couplings, commonly observed in practice, were a source of significant local inner anisotropy, resulting in dangerous parametric resonances and instability of the entire rotor-shaft system. The findings of the sensitivity analysis obtained for subsequent eigenvibration modes of this rotor-shaft system proved to be very helpful in identifying the most probable synchronous excitation sources among the possible types of rotor unbalance and shaft misalignments. Finally, the results of the qualitative tests carried out in this paper have been confirmed by multi-fault damage investigations, in which all the imperfections considered here were treated as uncertain interval quantities. Using the findings of this study, a diagnostic system for such a machine will be built.

REFERENCES

[1] K. Nandakumar and A. Chatterjee, "Nonlinear secondary whirl of an overhung rotor", in *Proc. R. Soc. A.*, vol. 466, pp. 283–301, 2010, doi: 10.1098/rspa.2009.0262.

[2] O. Cakmak and K.Y. Sanliturk, "A dynamic model of an overhung rotor with ball bearings", in *Proc. Inst. Mech. Eng., Part K: J. Multi-body Dyn.*, vol. 255, no. 4, pp. 310–321, 2011, doi: 10.1177/1464419311408949.

[3] Ch. Fu, X. Ren, Y. Yang, and W. Qin, "Dynamic response analysis of an overhung rotor with interval uncertainties", *Nonlinear Dyn.*, vol. 89, pp. 2115–2124, 2017, doi: 10.1007/s11071-017-3573-3.

[4] E. Chipato, A.D. Shaw, and M.I. Friswell, "Frictional effects on the Nonlinear Dynamics, of an overhung rotor", *Commun. Nonlinear Sci. Numer. Simul.*, vol. 78, p. 104875, 2019.

[5] ISO 1940/1, "*Balance Quality Requirements of Rigid Rotors*", International Organization for Standardization, 2003.

[6] K.M. Al-Hussain and I. Redmond, "Dynamic response of two rotors connected by rigid mechanical coupling with parallel misalignment", *J. Sound Vib.*, vol. 249, no. 3, pp. 483–498, 2002.

[7] K.M. Al-Hussain, "Dynamic stability of two rigid rotors connected by a flexible coupling with angular misalignment", *J. Sound Vib.*, vol. 266, no. 2, pp. 217–234, 2002.

[8] A.W. Lees, "Misalignment in rigidly coupled rotors", *J. Sound Vib.*, vol. 305, pp. 261–271, 2007.

[9] I. Redmond, "Study of a misaligned flexibly coupled shaft system having nonlinear bearings and cyclic coupling stiffness – Theoretical model and analysis", *J. Sound Vib*., vol. 329, pp. 700–720, 2010.

[10] J. Didier, J.-J. Sinou and B. Faverjon, "Study of the nonlinear dynamic response of a rotor system with faults and uncertainties", *J. Sound Vib*., vol. 331, pp. 671–703, 2012.

[11] P. Pennacchi, A. Vania, and S. Chatterton, "Nonlinear effects caused by coupling misalignment in rotors equipped with journal bearings", *Mech. Syst. Signal Process.*, no.30, pp. 306–322, 2012.

[12] A. Muszyńska, Ch.T. Hatch, and D.E. Bently, "Dynamics of anisotropically supported rotors", *Int. J. Rotating Mach.*, vol. 3, no. 2, pp. 133–142, 1997.

[13] J. Malta, "Investigation of anisotropic rotor with different shaft orientation", Doctoral Thesis, Darmstadt University of Technology, Department of Machinery Construction, D 17, Darmstadt, 2009.

[14] T. Szolc, P. Tauzowski, R. Stocki, and J. Knabel, "Damage identification in vibrating rotor-shaft systems by efficient sampling approach", *Mech. Syst. Signal Process.*, vol. 23, pp. 1615–1633, 2009.

[15] T. Szolc, "On the discrete-continuous modeling of rotor systems for the analysis of coupled lateral-torsional vibrations", *Int. J. Rotating Mach.*, vol. 6, no. 2, pp. 135–149, 2000.

[16] T. Szolc, K. Falkowski, M. Henzel, and P. Kurnyta-Mazurek, "The determination of parameters for a design of the stable electro-dynamic passive magnetic support of a high-speed flexible rotor", *Bull. Pol. Acad. Sci. Tech. Sci.*, vol. 67, no. 1, pp. 91–105, 2019.

[17] A. Pręgowska, R. Konowrocki, and T. Szolc, "On the semi-active control method for torsional vibrations in electro-mechanical systems by means of rotary actuators with a magneto-rheological fluid", *J. Theor. Appl. Mech.*, vol. 51, no. 4, pp. 979–992, 2013.

[18] R. Lasota, R. Stocki, P. Tauzowski, and T. Szolc, "Polynomial chaos expansion method in estimating probability distribution of rotor-shaft dynamic responses", *Bull. Pol. Acad. Sci. Tech. Sci.*, vol. 63, no. 1, pp. 413–422, 2015.

[19] Y. Ma, Z. Liang, M. Chen, and J. Hong, "Interval analysis of rotor dynamic response with uncertain parameters", *J. Sound Vib*., vol. 332, pp. 3869–3880, 2013.

[20] Z. Qiu and X. Wang, "Parameter perturbation method for dynamic responses of structures with uncertain-but-bounded parameters based on interval analysis", *Int. J. Solids Struct.*, vol. 42, pp. 4958–4970, 2005.

[21] Ch. Fu, Y. Xu, Y. Yang, K. Lu, F. Gu, and A. Ball, "Response analysis of an accelerating unbalanced rotating system with both random and interval variables", *J. Sound Vib*., vol. 466, p. 115047, 2020. https://doi.org/10.1016/j.jsv.2019.115047.